Solvation Structure and UV-Visible Absorption Spectra of the Nitrate Anion at the Air-Ice Interface by First Principles Molecular Simulations

Margaret L. Berrens,[†] Zekun Chen,[†] Kam-Tung Chan,[†] Cort Anastasio,[‡] and Davide Donadio[*,†]

[†]*Department of Chemistry, University of California Davis, One Shields Ave. Davis, CA, 95616.*

[‡]*Department of Land, Air, and Water Resources, University of California Davis, One Shields Ave. Davis, CA, 95616.*

E-mail: ddonadio@ucdavis.edu

Abstract

Nitrate is a significant contaminant in Polar snow. Its photolysis in environmental sunlight generates reactive nitrogen, which impacts the oxidative capacity of the atmosphere, influencing the fate and lifetimes of pollutants. The photolysis of nitrate can produce either NO_2 or NO_2^-, with recent experiments suggesting that the process is accelerated at the air-ice interface compared to the bulk solution. In this study, we employed multiscale modeling approaches to investigate the enhanced photoreactivity of nitrate at the ice surface in the presence of two different cations. We characterized the solvation shell of NO_3^- and explored its pairing with cations in water and ice using *ab initio* molecular dynamics and enhanced sampling. Molecular trajectories were

used to calculate light absorption spectra at different solvation conditions and finite temperature. Our analysis revealed that the pairing of nitrate with cations may alter the molar absorption coefficient of nitrate at the air-ice interface affecting the rate of photolysis observed in experiments of ammonium nitrate deposited on snow.

Keywords: Ammonium Nitrate, Nitric Acid, Light Absorption, Ice Surface, Ab Initio Molecular Dynamics, Time-Dependent Density Functional Theory.

Introduction

Snowpacks are active locations for numerous environmentally relevant chemical reactions.[1–3] Some of these reactions are enhanced because snowpacks contain small regions of disordered water molecules, known as bulk liquid-like regions (LLR), located within the ice matrix or quasi-liquid layers (QLL) at the surface of ice crystals.[2,4] These chemical reactions can release pollutants into the atmosphere, acting as sinks for contaminants. Among the several species involved in these reactions, nitrate is of particular interest. Nitrate (NO_3^-) is one of the most abundant anions on Earth and is found in snowpack due to continental, tropospheric, and stratospheric sources.[5,6] The photolysis of nitrate releases nitrogen oxides and nitrous acid into the atmospheric boundary layer, which can alter the lifetimes of gas-phase pollutants.[4,7] Additionally, the photolysis of nitrate in polar regions acts as a source of near-surface ozone and hydroxyl radicals into the atmospheric boundary layer, which then affects oxidative capacity.[8] For these reasons, understanding nitrate reactivity is essential for advancing snow and atmospheric chemistry.

Nitrate photolysis upon irradiation with UV light with wavelengths above 280 nm can proceed via two channels:

$$NO_3^- + h\nu \longrightarrow NO_2 + {}^{\bullet}O^- \quad (1)$$

$$NO_3^- + h\nu \longrightarrow NO_2^- + O(^3P) \quad (2)$$

Previous experiments have found that nitrate photolysis in LLR of ice behaves similarly to that of a supercooled solution, and the two channels have similar quantum yield.[7] Conversely, the turnover for channel (2) becomes three times higher when nitrate is solvated at the air-ice interface than in water.[9]

While an increase in quantum yield is usually considered the primary factor for the enhanced reactivity, a higher molar absorption coefficient of nitrate at the air-ice interface could further enhance nitrate photochemistry. Former works suggest that the absorbance of nitrate in ice LLRs is similar to that in bulk solution.[7,10,11] However, surprisingly a recent study[12] reported a molar absorption coefficient at 308 nm at the air-ice interface that is nearly 50 times higher than in solution. Such a large variability in experimental results may be ascribed to the difficulties of measuring UV-visible absorption spectra at low concentrations, comparable to environmental abundances. Molecular modeling allows one to overcome these issues as it provides an atomistic insight into the solvation environment of ions and small molecules at water and ice surfaces and may be used to compute absorption spectra in the limit of infinite dilution.[13–15]

In this article, we use first-principles molecular dynamics (FPMD) simulations and a multimodel approach to investigate the solvation shell and compute the UV-visible absorption spectra of nitrate at the air-ice interface and in water. We also investigate the effect of pairing with ammonium, an environmentally abundant counter ion often used in experiments, on the molar absorption coefficient of NO_3^-. Our multimodel approach combines density functional theory (DFT) based FPMD to sample the configurations of the ions in the solvation environment at finite temperature, and time-dependent density functional theory (TDDFT) to compute the UV-visible absorption spectra.[16–20] This method has been previously employed to assess the impact of the bathochromic shift in the UV-visible absorption spectra on the photolysis rates of organic pollutants at the air-ice interface.[3,21,22] Here we investigate the effect of the solvation environment by comparing bulk solution to

the air-ice interface while considering the effect of two common sources of nitrate on snowpack: nitric acid (HNO_3), and ammonium nitrate (NO_3^-/NH_4^+). The main goal is to test the hypothesis that the molar absorption coefficient of nitrate may be enhanced at the air-ice interface due to either solvatochromic shift or the formation of aggregates. The choice of modeling nitric acid and ammonium nitrate in these two solvation environments is motivated by both their broad environmental relevance and the availability of experimental data. Specifically, not only NO_3^-/NH_4^+ is used in several reference experiments,[9] but it is relevant beyond polar atmospheric chemistry, as HNO_3 and ammonia react in the gas phase to form solid particulate which is a major contributor to urban smog.[23] Furthermore, we work under the assumption that the structure of the solvation environment of NO_3^- in LLR is similar to that in bulk water at room temperature, whereas it is unlikely to have NO_3^- incorporated in crystalline bulk ice.[24] We find that the lowest energy band in the absorption spectra of all four systems does not exhibit any shift in the peak wavelength of absorption. However, the proximity of ammonium species at ice surfaces influences the molar absorption coefficient of nitrate, suggesting that clustering at the air-ice interface may affect light absorption and the photolysis of nitrate.

Computational Methods

Our sequential multiscale approach comprises the following steps: (i) classical molecular dynamics (MD) simulations provide a starting point for FPMD simulations; (ii) *ab initio* Well-tempered metadynamics[25] (MTD) simulations are used to sample the free energy landscape of the system for ions pairing; (iii) FPMD simulations refine the structure of the solvation shell and provide molecular configurations to compute UV-visible absorption spectra at finite temperature; (iv) TDDFT is used to compute the absorption spectra of the ions with a hybrid solvation model including their first solvation shell of explicit water molecules and a conductor-like polarizable continuum embedding (CPCM).[26]

Classical Molecular Dynamics

Classical MD simulation models were used to equilibrate the bulk solution and ice models of water. The bulk aqueous system consisted of 200 water molecules in a cubic simulation box (18.27 Å) with periodic boundary conditions (PBC) along all three dimensions. The equations of motion are integrated with the velocity Verlet algorithm with a time step of 0.5 fs. Simulations are carried out in the constant volume canonical ensemble (NVT), where the temperature is controlled by stochastic velocity rescaling[27] with a relaxation time of 1 ps, and long-range electrostatics are computed using the particle–particle/particle–mesh solver (PPPM).[28] MD simulations are performed using the LAMMPS package.[29] Water molecules are modeled using the fixed-charge TIP4P/Ice force field, which was parameterized to reproduce the experimental melting temperature of ice at ambient conditions, and it accurately reproduces the equations of state of water and ice near the melting temperature and at mild supercooling.[30]

For the air-ice interface, a proton-disordered hexagonal ice model containing 192 water molecules was generated using a Monte Carlo procedure to minimize the total electric dipole, and it was cut into a slab of 20 Å thick along the basal plane.[31] The orthorhombic simulation box measures $18.000 \times 15.590 \times 90.000$ Å^3 and periodic boundary conditions (PBC) are applied in all three directions. To avoid finite-size artifacts, periodic images of the slab are separated by ~ 70 Å vacuum along the z direction. The system was equilibrated for 10 ns at 263 K to obtain a stable QLL at the surface. The QLL is about two ice bilayers thick at both surfaces, in agreement with previous experimental observations and MD simulations.[32,33]

First-Principles Molecular Dynamics

FPMD simulations of several tens of picoseconds are performed for molecules in aqueous solution and at the air–ice interface. The purpose of these simulations is to attain a clearer picture of the dynamical hydrogen bonding network and to sample the configuration of the solvated molecule with a computational framework consistent with that used for the excited

state calculations. DFT-based FPMD simulations were carried out using the Quickstep approach implemented in the CP2K 8.2 package,[34,35] employing the Perdew–Burke–Ernzerhof (PBE) generalized gradient approximation (GGA) for the exchange and correlation (XC) functional[36] with D3 dispersion corrections.[37] Valence Kohn–Sham orbitals are expanded on a double-ζ localized basis set[38] in real space, and core states are treated implicitly using Goedecker–Teter–Hutter pseudopotentials.[39] Plane waves up to a cutoff energy of 300 Ry are used as a basis set for the density in reciprocal space. Using the aqueous and ice systems generated with classical MD and the aforementioned empirical force fields, the nitrate molecules and their counterions were placed at the surface and in the bulk. Eventually, using CP2K, the systems were equilibrated for 10 ps at the target temperature, followed by 70 ps long production runs in the constant volume canonical ensemble (NVT) where the temperature is controlled by stochastic velocity rescaling with a relaxation time of 1 ps.[27] Aqueous solutions were run at room temperature (300 K) and ice slabs at 263 K. In these simulations, hydrogen atoms were replaced with deuterium, thus allowing a relatively large timestep of 0.5 fs to integrate the equations of motion. The structural properties reported in the results section, including density profiles, density maps, radial distribution functions (RDF), and coordination numbers, are calculated averaging over 1400 frames taken every 50 fs for each 70 ps trajectory. Uncertainties are computed as the standard deviation over seven 10-ps-long blocks into which each trajectory is split. 800 statistically independent molecular configurations were extracted from each trajectory to compute UV–visible absorption spectra with the ensemble method.[19,20]

The necessity to run long simulations, of the order of several hundreds of ps, for systems containing up to 192 water molecules limits our choice of XC functional to semilocal GGA. Several studies compared the accuracy of various XC functionals when modeling water, showing that standard GGA functionals lead to substantial overstructuring of the liquid and a large underestimate of its equilibrium density.[40–43] However, the inclusion of dispersion corrections drastically improves the description of liquid water at nearly no additional

computational cost.[40,44,45]

The recently developed meta-GGA strongly-constrained and appropriately-normed (SCAN) functional[46] has been found to accurately capture density-driven differences between water and hexagonal and ice, as well as the structural, electronic, and dynamic properties of liquid water.[47] To provide independent validation of our simulation approach, we have computed the structural properties of the solvation shell of NO_3^- from FPMD using SCAN. RDFs were obtained from 10 ps production runs, starting from 5 ps equilibration.

Metadynamics Simulations

To explore efficiently the free energy surface of ammonium nitrate deposited on ice, and investigate the likelihood of ion pairing and deprotonation of ammonium, we employed well-tempered metadynamics.[25] Metadynamics is an enhanced sampling method where a history-dependent bias potential $V(s)$ is constructed on the fly as a function of the atomic trajectory via a restricted number of collective variables (CVs), $s = s(R)$ expressed as a function of the coordinates of the system (R). Collective variables are low dimensional descriptors of molecular structure. The fluctuations on the CVs can be gradually enhanced, allowing for large energy barriers to be overcome and rare events to take place in reasonable computational time. In the well-tempered version a Gaussian $G(s, s_k)$ centered at a visited point (s_k) is added periodically to the potential:

$$V_n(s) = \sum_{k=1}^{n} e^{\beta/(\gamma-1)V_{k-1}(s_k)} G(s, s_k) \tag{3}$$

where $\beta = 1/k_B T$, $\gamma > 1$ is the bias factor, and $G(s, s_k) = We^{\frac{-||s-s_k||^2}{2\sigma^2}}$ is a Gaussian function centered at the instantaneous position s_k, where W is the initial height and σ is the width of the Gaussian. FPMD was performed using CP2K, as described in the previous section, and the well-tempered metadynamics was implemented using PLUMED 2.7.[48] During the metadynamics runs, the Gaussians were added every 50 fs. A bias factor of $\gamma = 10$ was used.

Metadynamics is known to work especially well in terms of computational time and accuracy when the free energy surface is represented in a space of two or more collective variables.[49,50] Since we were interested in the dissociation of ammonium as well as the likelihood of the nitrate and the ammonia/ammonium pairing together throughout the trajectory, we used the following two collective variables: (i) the distance between the nitrogen atoms of the nitrate, and (ii) ammonium and the coordination number of the nitrogen and bonded hydrogen atoms in the ammonium molecule. The coordination number between atoms A (the nitrogen of the ammonium) and atoms B (the hydrogens of the ammonium) is defined as:

$$CN_{AB} = \sum_{i \in A} \sum_{j \in B} s_{ij}, \tag{4}$$

where s_{ij} is a switching function and is defined as:

$$s_{ij} = \frac{1 - (\frac{r_{ij}}{r_0})^n}{1 - (\frac{r_{ij}}{r_0})^m} \tag{5}$$

r_{ij} is the distance between the two atoms, and n and m are set equal to 6 and 12, respectively. The Gaussian widths used are 0.2 Å and 0.05 for the nitrogen distance and coordination number respectively. The Gaussians added to form the history-dependent potential had an initial height of 1.0 kJ/mol, at 120 ps the height was increased to 2.5 kJ/mol, then a final increase at 140 ps to 5.0 kJ/mol, which was then damped throughout the simulation. At convergence, the relative free energy can be calculated from the applied biases:[25]

$$F(s) = -\frac{\gamma}{\gamma - 1} V(s) \tag{6}$$

The convergence of the well-tempered metadynamics simulation was evaluated by the diffusion of CVs and the average error of the relative free energy against time through block analysis.[51]

UV-Visible Absorption Spectra Calculations

Nitrate absorption spectra at finite temperature are calculated as the ensemble average of 800 vertical excitation energies from the individual frames extracted from the FPMD trajectories. For each frame, vertical excitation energies and oscillator strengths were computed using TDDFT, with the CAM-B3LYP hybrid density functional.[52] CAM-B3LYP has been shown to accurately model excited states of nitrate anion under solvation.[53,54] All the TDDFT calculations were performed using a triple-ζ valence polarized Karlsruhe (def2-TZVP) basis set along with the resolution of identity approximation for the Coulomb and exchange integrals.[55] The UV-visible spectra are obtained from the Gaussian envelopes with an empirical broadening width σ of 0.027 eV. UV-Visible absorption spectra calculations were performed using ORCA 5.0.1 package.[56]

To account for the effect of ion pairing at the surface of ice, we have computed separately the absorption spectra of the molecular complexes made of NO_3^- paired with either NH_4^+ or NH_3, treating ammonium/ammonia explicitly together with the water solvation shell. These systems are embedded in a hybrid solvation model, where the first two solvation shells of NO_3^-, which correspond to 12 water molecules, are treated explicitly, and the long-range screening is accounted for by the CPCM polarizable implicit solvent, with a static dielectric constant of 80.3 and refractive index 1.33.[26] Svoboda, et. al,[53] calculated the electronic absorption spectra of isolated and solvated nitrate anion in the UV region and found that adding beyond 10 explicit water molecules does not modify the predicted spectra.

Results and Discussions

In the FPMD simulations in bulk water and at the air-ice interface, nitrate acid deprotonates within the first picosecond and diffuses away from the nitrate anion via hopping. The solvation environment of NO_3^- equilibrates within the first five picoseconds. The deprotonation of nitric acid in water and on ice by FPMD was reported in detail in previous works and our

simulations also saw picosecond time-scale ionization.[57–59] Additionally, upon deprotonation of the nitric acid we saw efficient proton transfer throughout the solution as well as at the quasi-liquid layer. In the simulations of ammonium nitrate in bulk solution, NH_4^+ remains in its ionic form and is sufficiently far from NO_3^- to consider the two ions non-interacting. Conversely, preliminary FPMD simulations of ammonium nitrate at the air-ice interface show that NH_4^+ and NO_3^- tend to aggregate spontaneously. For this system, we ran two independent simulations, starting with the two ions 5 Å and 10 Å apart. In the former case, the distance between the N atoms of NO_3^- and NH_4^+ fluctuates between 3 and 5.5 Å over the 70 ps of the simulation (Figure S1). In the latter case, the two ions rapidly approach and NH_4^+ deprotonates to NH_3. After 20 ps in which the N-N distance oscillates between 3.5 and 8 Å, the NO_3^-/NH_3 complex stabilizes at an average distance of 4.5–5 Å (Figure S2). The spontaneous formation of ammonia may be surprising at first glance as NH_4^+ has a pK_a of 9.3 in bulk water, but there is evidence that the equilibrium of protonation/deprotonation reactions is significantly altered at ice surfaces.[60,61]

Ion pairing on ice

To investigate the stability of the ion complexes and the deprotonation of ammonium to ammonia we use well-tempered metadynamics simulations,[25] and explore the free energy surface using two collective variables: the N-N distance between NO_3^- and NH_4^+, and the coordination number of ammonium with hydrogen defined in Eq. 4. Figure 1) shows the free energy surface (FES) as well as the coordination number and nitrogen distances throughout the metadynamics simulation. The average error of the FES is obtained from the diffusion of the CVs and block average analysis (Figure S3).[51] The average error on the FES converges to ~ 0.8 kJ/mol, and the maximum error is 2.2 kJ/mol in the regions of the CVs space that are sampled less frequently. These data show that at the air-ice interface, for the surface coverage considered, it is more favorable for nitrate to be fully separated from ammonium, which is preferentially protonated, similar to that of ammonium nitrate in bulk aqueous

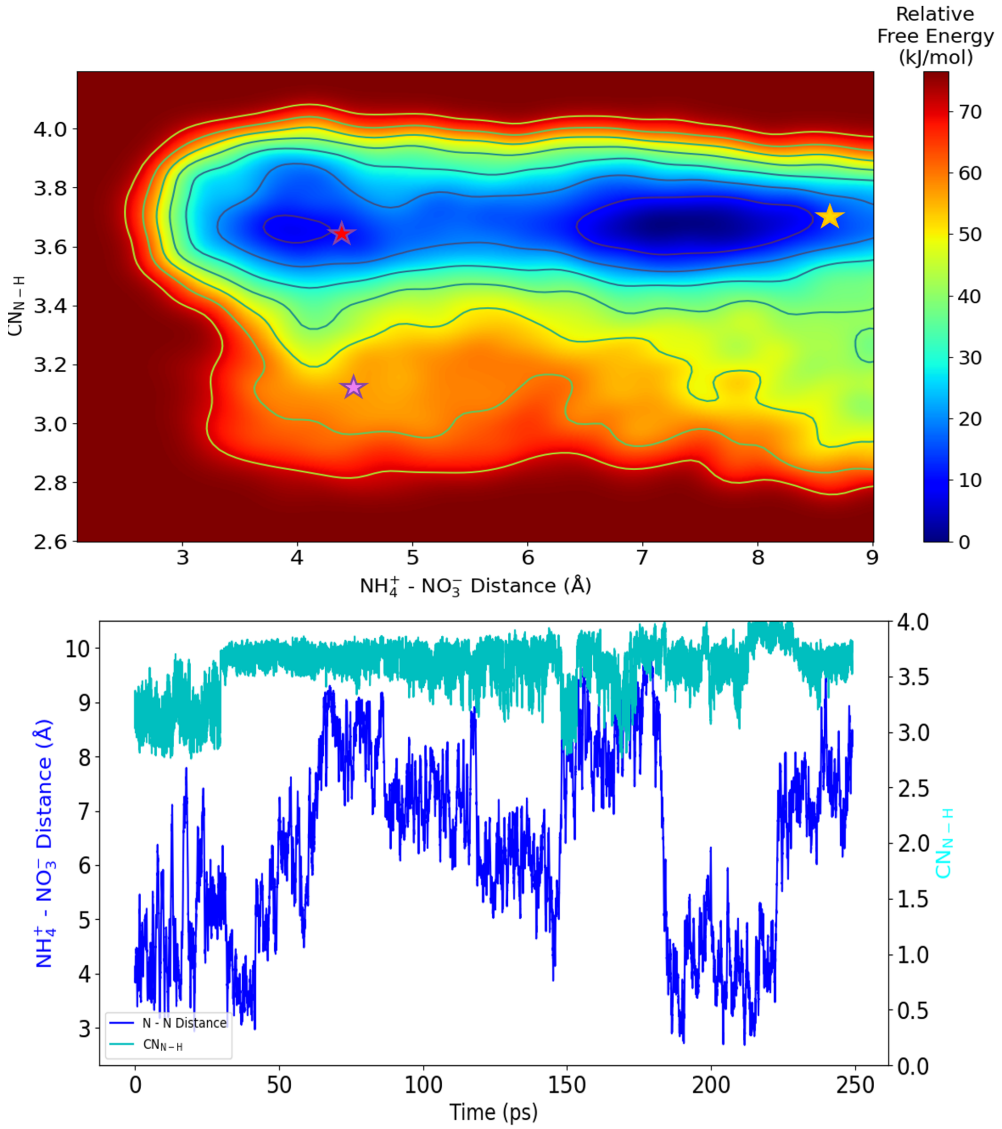

Figure 1: The free energy surface of ammonium nitrate at the air-ice interface at 263 K in the collective variables space defined by the coordination number of ammonium, and the distance between nitrogen atoms. Each of the stars represents the averaged values of the collective variables throughout their respective unbiased trajectories. The pink star is for the ammonia nitrate run, the red star is for the first ammonium nitrate run, and the yellow star is for the restarted ammonium nitrate run.

solution (white star in Fig. 1). However, configurations in which nitrate and ammonium are paired (N-N distance $\sim$ 4 Å, red star in Fig. 1) are metastable, and a low barrier of the order of the thermal energy separates the two free energy basins. The FES shows that ammonium deprotonation is more likely when the two ions are separated, whereas the nitrate-ammonia

complex (pink star in Fig. 1) is not thermodynamically stable. However, the unbiased FPMD runs suggest that even though according to the reconstructed free energy surface they are not the most probable scenarios, both the NO_3^-/NH_3 and NO_3^-/NH_4^+ complexes are long-lived at the air-ice interface over time scales of several tens of ps. The relatively favorable clustering of ammonia and ammonium with nitrate molecules at the ice surface can be explained by the fact that the hydration of ions leads to an increase in surface liquidity at the ice surface, which in turn creates a water-mediated attraction of ions, as observed previously.[62]

Figure S4 maps the path taken by our two sampled trajectories on the free energy surface and shows that neither of our starting configurations for the unbiased runs reached the minimum of the reconstructed free energy surface. So, we carried out a 20 ps long, unbiased, molecular dynamics run of ammonium nitrate at the air-ice interface - starting from a configuration extracted from the metadynamics simulation in which the ions are separated. In this unbiased run, ammonium nitrate stays protonated as ammonium, the two ions stay far apart, and the system remains within the global minimum basin of the FES (Figure S4).

Solvation shell structure

We first analyze the structure of the solvation shell of NO_3^- obtained from the deprotonation of nitric acid and from ammonium nitrate at the air-ice interface and in water. Before comparing the solvation structure of nitrate in water and at the air-ice interface, we observe that at the ice surface, NO_3^- is fully solvated in the QLL, as opposed to larger hydrophobic pollutants that float on top of the QLL (Figure 2ab).[21,22] However, when NO_3^- forms a complex with NH_4^+, the ion pair is located at the tail of the density profile. These differences in the QLL embedding lead to different solvation environments for NO_3^-, and influence its molar absorption coefficient, possibly influencing its molar absorption coefficient and photodissociation kinetics.

To investigate the solvation properties of nitrate in water and at the air-ice interface, we

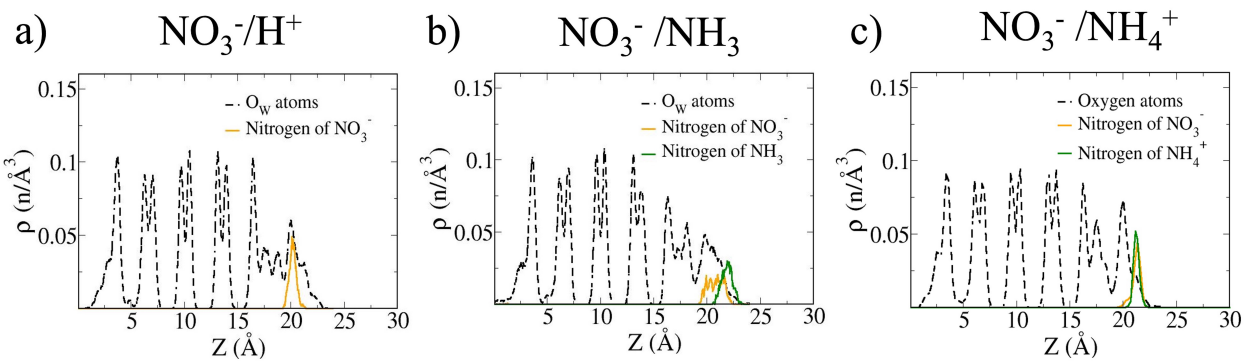

Figure 2: Oxygen atom density profiles of the two sampled ice systems for a) nitric acid, b) ammonia nitrate, c) ammonium nitrate.

computed the RDF, coordination numbers ($CN(R)$), and 3D density maps of NO_3^- from the FPMD runs discussed above. The solvation shell of NO_3^- is characterized by the hydrogen bonds between the oxygen atoms of the nitrate (O_n) and water (O_w and H_w). The O_n-H_w RDFs are reported in Figure 3. The RDFs for the other pairs of atoms on the nitrate anion and water are reported in Figure S5.

RDFs for the HNO_3 case were also computed using the SCAN functional (Figure S6). The solvation structures of NO_3^- in water computed using PBE-D3 and SCAN are consistent with one another, especially for the position and intensity of the nearest neighbors' peaks. Differences emerge in the intensity of the larger distance peaks, possibly also due to statistical uncertainties.

In the deprotonated nitric acid case (NO_3^-/H^+), the N_n-H_w, N_n-O_w, O_n-O_w, and O_n-H_w RDFs on ice are more structured than those in water. This is only partially due to the temperature difference between the two systems, but mostly to the more ordered structure of the QLL at the air-ice interface, in which NO_3^- is fully embedded. When the system is prepared from ammonium nitrate, the solvation shell of NO_3^- in aqueous solution is very similar to that of deprotonated nitric acid. At the ice surface, two different situations should be considered: (i) paired NO_3^-/NH_4^+, and (ii) paired NO_3^-/NH_3.

By comparing to the RDF of HNO_3 on ice, we see that when an ion complex is formed, in

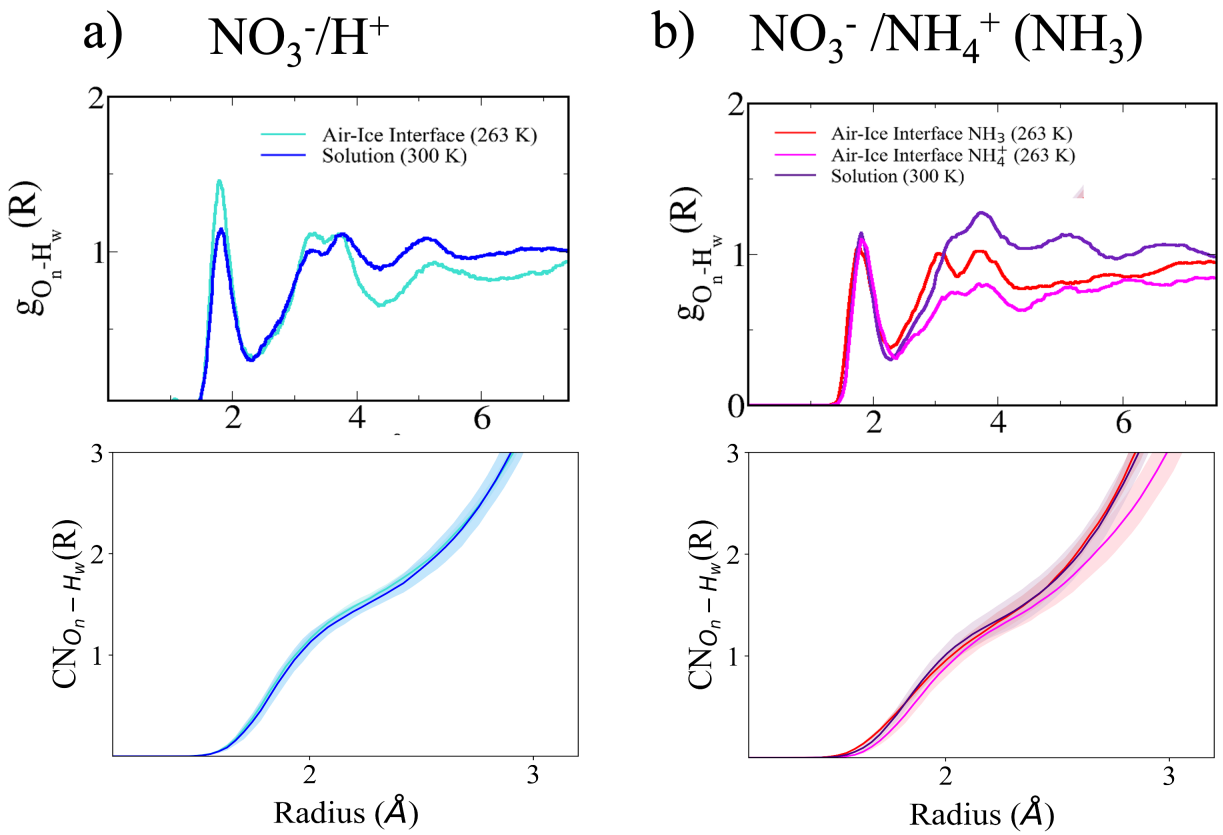

Figure 3: Radial distribution functions (g(r)) between the oxygen atoms on the nitrate and the hydrogens of the water for a) nitric acid and b) ammonium/ammonia nitrate obtained in solution and at the air-ice interface. Below the radial distribution functions are the corresponding coordination numbers (CN(R)) between the oxygen atoms on the nitrate and the hydrogens of the water, averaged over each 70 ps trajectory.

both cases, the solvation shell of NO_3^- on ice is partly disrupted. This leads to a lower first peak of the O_n-H_w and O_n-O_w RDFs, similar to that obtained for nitrate in bulk water at 300 K, while the structure of the RDF beyond the first solvation peak changes as a function of the presence and the protonation state of ammonium/ammonia. From these RDFs, we learn that in terms of solvation environment, there are slight differences between water and ice due to the more ordered structure of the quasi-liquid layer. However, if a counter ion is close enough to disrupt the first solvation shell then this leads to significant differences in the water structuring around the ion, which we will see below.

Figure 3(bottom panels) shows the coordination number between the oxygen atoms on

the nitrate and the hydrogen atoms of water ($CN_{O_n-H_w}(R)$), defined as the volume integral of the corresponding RDF up to a radius R.[1] The enhanced ordering of the solvation shell of NO_3^- on ice for the NO_3^-/H^+ results in a slightly increased average number of accepted hydrogen bonds per oxygen atom from 1.51±0.092 to 1.57±0.096 (Figure 3a). In turn, the disruption in the solvation shell of NO_3^- on ice for the NO_3^-/NH_4^+ results in a decrease of the average number of accepted hydrogen bonds per oxygen atom from 1.51±0.14 in solution to 1.45±0.12 NO_3^-/NH_3 on ice to 1.35±0.13 NO_3^-/NH_4^+ on ice (Figure 3b).

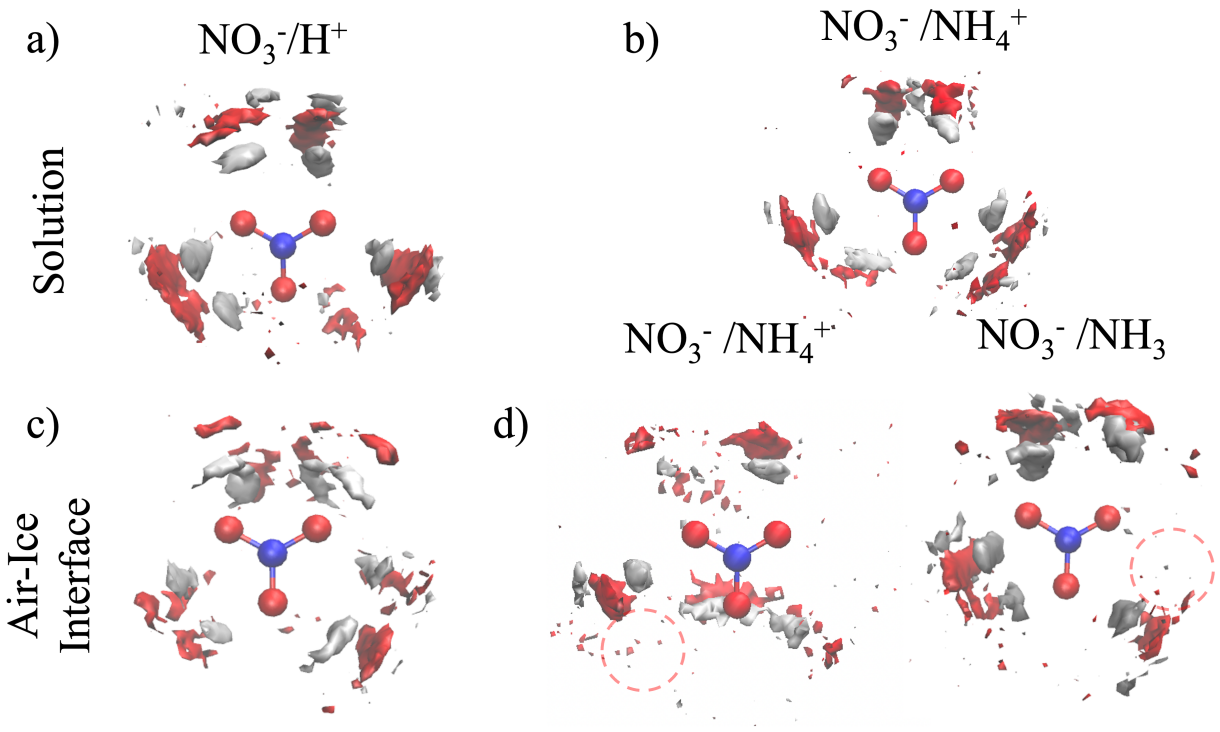

Figure 4: Three-dimensional density maps of the oxygen atoms of the water molecules and the hydrogen atoms of the water molecules surrounding the nitrate molecule for nitric acid (a. and c.) and ammonium/ammonia nitrate (b. and d.) in both solvation environments. Density maps were obtained by averaging over the 70 ps trajectories.

The three-dimensional density maps of the water surrounding the nitrates in each system are shown in Figure 4. Figure 4 a) b) and c) all exhibit similar water structuring around the nitrate. Figure 4 d) shows the water density around the nitrate at the air-ice interface paired with ammonium/ammonia. For the first three systems, there are two dis-

[1]This function should not be confused with coordination number CV used in the metadynamics runs.

tinct water-dense areas per oxygen of the nitrate due to the fluctuations in the location of water throughout the trajectory. However for Figure 4d) there are only four or five distinct water-dense areas. Looking further into this, the gap in water density is due to the presence of ammonium/ammonia as for both systems this molecule resides within 5 Å of NO_3^-. Additionally, since the ammonium nitrate complex floats at the surface of the QLL (see Fig. 2), the water distribution is on one side of the plane of the nitrate anion.

Even though less likely, nitrate can also form a hydrogen-bonded complex with ammonia. As there is no direct bond between NO_3^- and NH_3, the complex is stabilized by a hydrogen-bonding bridge of two water molecules (Figure S7). The first solvation shell of this complex exhibits a density gap in correspondence to the position of NH_3. In this case, the nitrate anion is deeper into the QLL, and the neighboring water molecules' density peaks in the plane of NO_3^-.

UV-visible light absorption

Hereafter, we explore the effect of the different solvation environments on the light absorption of nitrate. From each MD trajectory analyzed above, we calculated the UV-visible absorption spectrum at a finite temperature using the ensemble approach described in the methods section. The full spectra are displayed in Figure S8, while the most environmentally relevant lowest-energy band is shown in Figure 5). The spectra in Figure S8 exhibit a profound absorption band due to due to a $\pi \rightarrow \pi^*$ transition at 205 nm, followed by a minor absorption band related to a $n \rightarrow \pi^*$ transition at $\sim$ 300 nm.[63,64] The molar absorption coefficient (ε) of the $n \rightarrow \pi^*$ transition is several orders of magnitude smaller than ε from the $\pi \rightarrow \pi^*$ transition, as the former is forbidden by symmetry. However, finite-temperature distortion and the presence of cations and polar solvent molecules break the symmetry and result in a finite absorption band at the edge of the solar spectrum.[65–67]

The wavelength at the maximum absorptivity (λ_{max}) is between 305 and 307 nm, regardless of the solvation environment. In experiments, λ_{max} is at 301 and 303 nm for nitrate

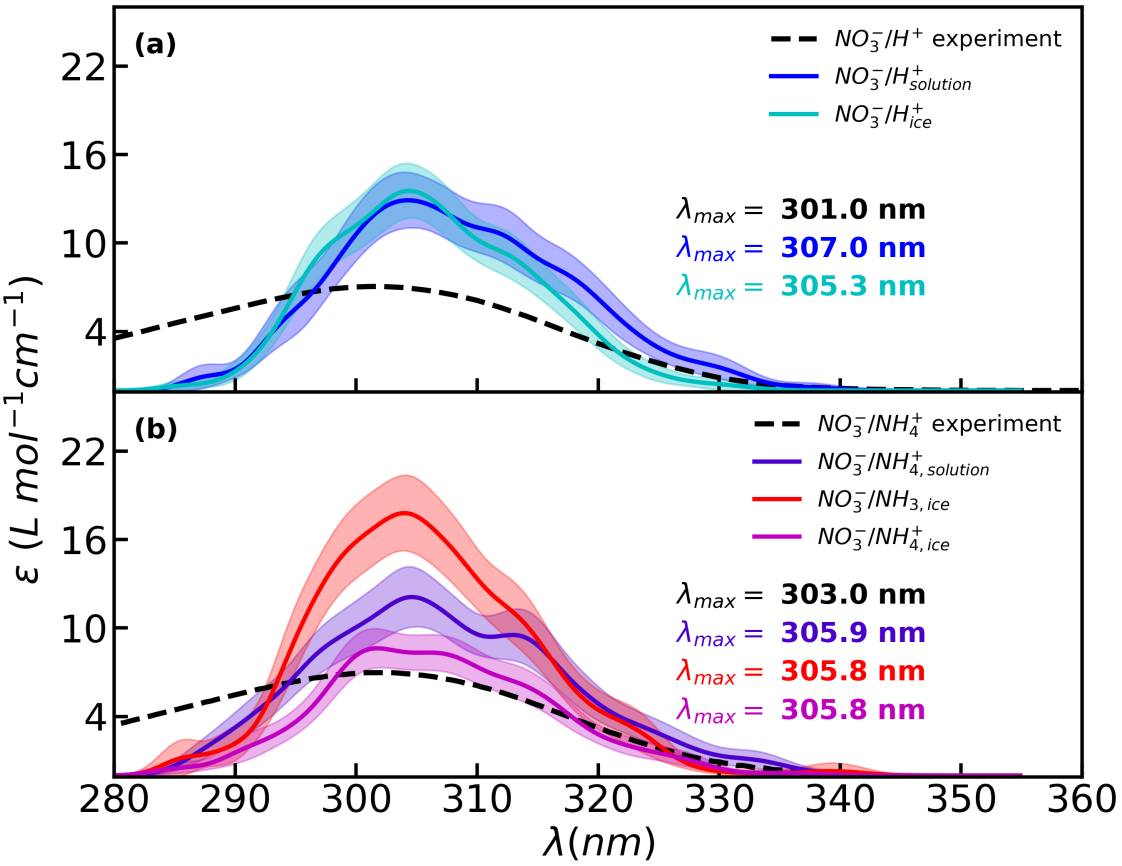

Figure 5: Absorption spectra for nitric acid (a) and ammonium/ammonia nitrate (b) in solution and on the air-ice interface obtained using TDDFT. λ_{max} values represent wavelengths of peak absorbance in the long-wavelength band. The black dashed line represents nitric acid (a) and ammonia nitrate (b) in an aqueous solution, both measured at 293.15 K. Fillings for each calculated spectra represent 95% confident interval derived from 800 single frame spectra.[7]

in aqueous solution originating from HNO_3[7] and NH_4NO_3, respectively.[68] For deprotonated HNO_3, we observe a slight blue shift of λ_{max} of $\sim$ 2 nm when nitrate is at the air-ice interface, whereas no shift in the peak position occurs for the NH_4NO_3 system. Such a small shift in λ_{max}, corresponding to excitation energy changes of about 30 meV, is far below the accuracy of our computational approach. Hence, we conclude that our calculations predict no significant solvatochromic shift for nitrate on ice. This result is consistent with UV-visible absorption measurements showing no shift for nitrate in liquid water and in a frozen

solution.[10,11]

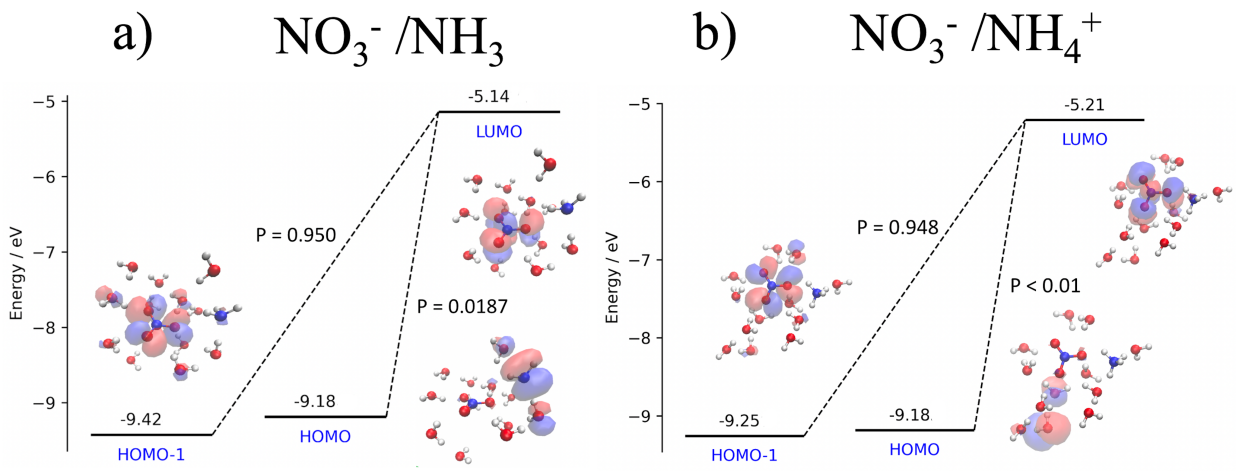

Figure 6: Two representative energy diagrams for the ammonia/ammonium nitrate at the air-ice interface. Values and molecular orbitals are from a sample frame used for the TDDFT calculations. The values on the lines connecting the HOMO and HOMO - 1 to the LUMO represent the weight P of the individual excitation to the S_1 state.

While we see no significant solvatochromic shift, the coupling with ammonium or ammonia affects the molar absorption coefficient of nitrate. The presence of ammonia leads to an enhancement of ε, in contrast with a reduction of ε induced by coupling with ammonium in Figure 5. In contrast, this change in ε was not seen experimentally between NO_3^-/NH_4^+ and HNO_3 in solution. Figure 6 shows the energy diagrams for two representative configurations of the NO_3^-/NH_3 (a) and the NO_3^-/NH_4^+ complexes on ice. In the first case, the ammonia provides an occupied state with energy quasi-degenerate with the HOMO of NO_3^-. This state provides a finite contribution to the $S_0 \rightarrow S_1$ excitation of the complex, thus enhancing the overall molar absorption coefficient. Conversely, NH_4^+ does not provide additional excitation channels, and its presence partly disrupts the first solvation shell of the nitrate anion, leading to a small decrease in the molar absorption coefficient.

Conclusions

We have used first-principles molecular dynamics to study the solvation shell of nitrate obtained by dissolving nitric acid and ammonium nitrate in an aqueous solution and at the air-ice interface. Additionally, we assessed the effect of different solvation environments on the UV-Visible absorption spectra, in particular for energies corresponding to the solar photon flux on Earth. These calculations indicate that the lowest-energy absorption band at ~ 305 nm does not undergo any significant solvatochromic shift when nitrate is deposited on ice rather than solvated in water, and the intensity of the absorption band is unchanged. These results stem from the observation that NO_3^- on ice is fully embedded in the QLL, and the structure of its solvation shell is very similar to that in bulk water.

Conversely, we observed that when ammonium nitrate is deposited on ice, NO_3^- can pair with NH_4^+, or even form a hydrogen-bonded complex with NH_3. In the case of NO_3^-/NH_4^+ pairing, our calculations predict a slightly attenuated molar absorption coefficient, whereas when a NO_3^-/NH_3 complex is formed the molar absorption coefficient of nitrate is enhanced roughly by a factor of 1.5. At the concentration of our simulations, corresponding to $0.3/\text{nm}^2$, the formation of aggregates of nitrate have a relatively low probability, but at higher concentrations and different pH conditions pairing of nitrate with ammonium or ammonia would become more relevant and affect light absorption. Nevertheless, while our results suggest that the formation of surface aggregates influences the photon uptake of nitrate, the computed variations of the molar absorption coefficient are relatively small compared to the enhancement of photolysis at the air-ice interface observed in experiments. It is then sensible to assume that such enhancement is mostly due to augmented quantum yields for either or both nitrate photodissociation channels. To achieve a full picture of nitrate photolysis, further modeling, and experimental work is needed to determine the quantum yield of the two nitrate photolysis channels at the air-ice interface and in bulk aqueous solutions.[69,70]

Conflicts of interest

There are no conflicts to declare.

Supporting Information

Coordination number definition, distance profile of ions in solution and at the air-ice interface, convergence of the relative free energy, path on free energy surface of unbiased trajectories, radial distribution functions of nitrate anion, distance profile of hydrogen bonds, convergence of absorption spectra.

Data availability

Data are available in the Materials Cloud Archive (www.materialscloud.org) with ID materialscloud:2023.115, doi:10.24435/materialscloud:4d-p4.

Acknowledgements

We are grateful to Ted Hullar and Aaron Lieberman for many valuable discussions and suggestions. We thank Fernanda Bononi, Wang-Yeuk Kong, and William Bro-Jørgenson for useful suggestions on the simulation setup and the calculation of the UV-visible spectra. This work is supported by the National Science Foundation under Grant No. 1806210 and No. 2305164.

References

(1) Dominé, F.; Shepson, P. B. Air-snow interactions and atmospheric chemistry. *Science* **2002**, *297*, 1506–1510.

(2) Bartels-Rausch, T.; Bergeron, V.; Cartwright, J. H.; Escribano, R.; Finney, J. L.; Grothe, H.; Gutiérrez, P. J.; Haapala, J.; Kuhs, W. F.; Pettersson, J. B., et al. Ice structures, patterns, and processes: A view across the icefields. *Rev. Mod. Phys.* **2012**, *84*, 885.

(3) Hullar, T.; Bononi, F. C.; Chen, Z.; Magadia, D.; Palmer, O.; Tran, T.; Rocca, D.; Andreussi, O.; Donadio, D.; Anastasio, C. Photodecay of guaiacol is faster in ice, and even more rapid on ice, than in aqueous solution. *Environ. Sci.: Process. Impacts* **2020**, *22*, 1666–1677.

(4) Beine, H. J.; Dominé, F.; Simpson, W.; Honrath, R. E.; Sparapani, R.; Zhou, X.; King, M. Snow-pile and chamber experiments during the Polar Sunrise Experiment 'Alert 2000': exploration of nitrogen chemistry. *Atmos. Environ.* **2002**, *36*, 2707–2719.

(5) Shi, G.; Hastings, M. G.; Yu, J.; Ma, T.; Hu, Z.; An, C.; Li, C.; Ma, H.; Jiang, S.; Li, Y. Nitrate deposition and preservation in the snowpack along a traverse from coast to the ice sheet summit (Dome A) in East Antarctica. *Cryosphere* **2018**, *12*, 1177–1194.

(6) Chen, Q.; Edebeli, J.; McNamara, S. M.; Kulju, K. D.; May, N. W.; Bertman, S. B.; Thanekar, S.; Fuentes, J. D.; Pratt, K. A. HONO, Particulate Nitrite, and Snow Nitrite at a Midlatitude Urban Site during Wintertime. *ACS Earth Space Chem.* **2019**, *3*, 811 – 822.

(7) Chu, L.; Anastasio, C. Quantum yields of hydroxyl radical and nitrogen dioxide from the photolysis of nitrate on ice. *J. Phys. Chem. A* **2003**, *107*, 9594–9602.

(8) Chu, L.; Anastasio, C. Temperature and wavelength dependence of nitrite photolysis in frozen and aqueous solutions. *Environ. Sci. Technol.* **2007**, *41*, 3626–3632.

(9) Benedict, K. B.; McFall, A. S.; Anastasio, C. Quantum yield of nitrite from the photolysis of aqueous nitrate above 300 nm. *Environ. Sci. Technol.* **2017**, *51*, 4387–4395.

(10) Dubowski, Y.; Colussi, A.; Boxe, C.; Hoffmann, M. Monotonic increase of nitrite yields in the photolysis of nitrate in ice and water between 238 and 294 K. *J. Phys. Chem. A* **2002**, *106*, 6967–6971.

(11) Matykiewiczova, N.; Kurková, R.; Klánová, J.; Klán, P. Photochemically induced nitration and hydroxylation of organic aromatic compounds in the presence of nitrate or nitrite in ice. *J. Photochem. Photobiol.* **2007**, *187*, 24–32.

(12) Zhu, C. Z.; Xiang, B.; Chu, L. T.; Zhu, L. 308 nm Photolysis of Nitric Acid in the Gas Phase, on Aluminum Surfaces, and on Ice Film. *J. Phys. Chem. A* **2010**, *114*, 2561–2568.

(13) Epstein, S. A.; Shemesh, D.; Tran, V. T.; Nizkorodov, S. A.; Gerber, R. B. Absorption Spectra and Photolysis of Methyl Peroxide in Liquid and Frozen Water. *J. Phys. Chem. A* **2009**, *116*, 6068– 6077.

(14) Gopalakrishnan, S.; Jungwirth, P.; Tobias, D. J.; Allen, H. C. Air-Liquid Interfaces of Aqueous Solutions Containing Ammonium and Sulfate: Spectroscopic and Molecular Dynamics Studies. *J. Phys. Chem. B* **2005**, *109*, 8861– 8872.

(15) Vácha, R.; Cwiklik, L.; Řezáč, J.; Hobza, P.; Jungwirth, P.; Valsaraj, K.; Bahr, S.; Kempter, V. Adsorption of Aromatic Hydrocarbons and Ozone at Environmental Aqueous Surfaces. *J. Phys. Chem. A* **2008**, *112*, 94942– 4950.

(16) Blase, X.; Duchemin, I.; Jacquemin, D. The Bethe–Salpeter equation in chemistry: relations with TD-DFT, applications and challenges. *Chem. Soc. Rev.* **2018**, *47*, 1022–1043.

(17) Casida, M. E. Time-dependent density-functional theory for molecules and molecular solids. *J. Mol. Struct.: THEOCHEM* **2009**, *914*, 3–18.

(18) Burke, K.; Werschnik, J.; Gross, E. Time-dependent density functional theory: Past, present, and future. *J. Chem. Phys.* **2005**, *123*, 062206.

(19) Timrov, I.; Andreussi, O.; Biancardi, A.; Marzari, N.; Baroni, S. Self-consistent continuum solvation for optical absorption of complex molecular systems in solution. *J. Chem. Phys.* **2015**, *142*, 034111.

(20) Timrov, I.; Micciarelli, M.; Rosa, M.; Calzolari, A.; Baroni, S. Multimodel approach to the optical properties of molecular dyes in solution. *J. Chem. Theory Comput.* **2016**, *12*, 4423–4429.

(21) Bononi, F.; Chen, Z.; Rocca, D.; Andreussi, O.; Hullar, T.; Anastasio, C.; Donadio, D. Bathochromic Shift in the UV–Visible Absorption Spectra of Phenols at Ice Surfaces: Insights from First-Principles Calculations. *J. Phys. Chem. A* **2020**, *124*, 9288–9298.

(22) Hullar, T.; Tran, T.; Chen, Z.; Bononi, F.; Palmer, O.; Donadio, D.; Anastasio, C. Enhanced photodegradation of dimethoxybenzene isomers in/on ice compared to in aqueous solution. *Atmos. Chem. and Phys.* **2022**, *22*, 5943–5959.

(23) Wang, M. et al. Rapid growth of new atmospheric particles by nitric acid and ammonia condensation. *Nature* **2020**, *581*, 184–189, Number: 7807 Publisher: Nature Publishing Group.

(24) Wren, S. N.; Donaldson, D. J. Exclusion of Nitrate to the Air-Ice Interface During Freezing. *J. Chem. Phys. Lett.* **2011**, *2*, 1967–1971.

(25) Barducci, A.; Bussi, G.; Parrinello, M. Well-tempered metadynamics: a smoothly converging and tunable free-energy method. *Phys. Rev. Lett.* **2008**, *100*, 020603.

(26) Barone, V.; Cossi, M. Quantum calculation of molecular energies and energy gradients in solution by a conductor solvent model. *J. Phys. Chem. A.* **1998**, *102*, 1995–2001.

(27) Bussi, G.; Donadio, D.; Parrinello, M. Canonical sampling through velocity rescaling. *J. Chem. Phys.* **2007**, *126*, 014101.

(28) Eastwood, J. W.; Hockney, R. W.; Lawrence, D. N. P3M3DP-the three-dimensional periodic particle-particle/particle-mesh program. *Comput. Phys. Commun.* **1984**, *35*, C–618, Num Pages: C-619.

(29) Plimpton, S. Fast parallel algorithms for short-range molecular dynamics. *J. Comp. Phys.* **1995**, *117*, 1–19.

(30) Abascal, J.; Sanz, E.; García Fernández, R.; Vega, C. A potential model for the study of ices and amorphous water: TIP4P/Ice. *J. Chem. Phys.* **2005**, *122*, 234511.

(31) Buch, V.; Sandler, P.; Sadlej, J. Simulations of H2O Solid, Liquid, and Clusters, with an Emphasis on Ferroelectric Ordering Transition in Hexagonal Ice. *J. Phys. Chem. B* **1998**, *102*, 8641–8653.

(32) Kling, T.; Kling, F.; Donadio, D. Structure and dynamics of the quasi-liquid layer at the surface of ice from molecular simulations. *J. Phys. Chem. C* **2018**, *122*, 24780–24787.

(33) Sánchez, M. A.; Kling, T.; Ishiyama, T.; van Zadel, M.-J.; Bisson, P. J.; Mezger, M.; Jochum, M. N.; Cyran, J. D.; Smit, W. J.; Bakker, H. J., et al. Experimental and theoretical evidence for bilayer-by-bilayer surface melting of crystalline ice. *Proc. Natl. Acad. Sci. U.S.A.* **2017**, *114*, 227–232.

(34) VandeVondele, J.; Krack, M.; Mohamed, F.; Parrinello, M.; Chassaing, T.; Hutter, J. Quickstep: Fast and accurate density functional calculations using a mixed Gaussian and plane waves approach. *Comp. Phys. Commun.* **2005**, *167*, 103–128.

(35) Iannuzzi, M.; Laio, A.; Parrinello, M. Efficient exploration of reactive potential energy surfaces using Car-Parrinello molecular dynamics. *Phys. Rev. Lett.* **2003**, *90*, 238302.

(36) Perdew, J. P.; Burke, K.; Ernzerhof, M. Generalized gradient approximation made simple. *Phys. Rev. Lett.* **1996**, *77*, 3865.

(37) Grimme, S.; Antony, J.; Ehrlich, S.; Krieg, H. A consistent and accurate ab initio parametrization of density functional dispersion correction (DFT-D) for the 94 elements H-Pu. *J. Chem. Phys.* **2010**, *132*, 1504.

(38) VandeVondele, J.; Hutter, J. Gaussian basis sets for accurate calculations on molecular systems in gas and condensed phases. *J. Chem. Phys.* **2007**, *127*, 114105.

(39) Goedecker, S.; Teter, M.; Hutter, J. Separable dual-space Gaussian pseudopotentials. *Phys. Rev. B* **1996**, *54*, 1703.

(40) Zhou, K.; Qian, C.; Liu, Y. Quantifying the Structure of Water and Hydrated Monovalent Ions by Density Functional Theory-Based Molecular Dynamics. *J. Phys. Chem. B* **2022**, *126*, 10471–10480.

(41) Gillan, M. J.; Alfe, D.; Michaelides, A. Perspective: How good is DFT for water? *J. Chem. Phys.* **2016**, *144*, 130901.

(42) Lin, I.-C.; Seitsonen, A. P.; Tavernelli, I.; Rothlisberger, U. Structure and Dynamics of Liquid Water from ab Initio Molecular Dynamics—Comparison of BLYP, PBE, and revPBE Density Functionals with and without van der Waals Corrections. *J. Chem. Theory Comput.* **2012**, *8*, 3902–3910.

(43) Bankura, A.; Karmakar, A.; Carnevale, V.; Chandra, A.; Klein, M. L. K. Structure, Dynamics, and Spectral Diffusion of Water from First-Principles Molecular Dynamics. *J. Phys. Chem. C* **2014**, *118*, 29401–29411.

(44) Morawietz, T.; Singraber, A.; Dellago, C.; Behler, J. How van der Waals interactions determine the unique properties of water. *Proc Natl Acad Sci USA* **2016**, *113*, 8368–8373.

(45) Wang, J.; Roman-Perez, G.; Soler, J. M.; Artacho, E.; Fernandez-Serra, M. V. Density, structure, and dynamics of water: The effect of van der Waals interactions. *J. Chem. Phys.* **2011**, *134*, 024516.

(46) Sun, J.; Ruzsinszky, A.; Perdew, J. P. Strongly Constrained and Appropriately Normed Semilocal Density Functional. *Phys. Rev. Lett.* **2015**, *115*, 036402.

(47) Chen, M.; Ko, H.; Remsing, R. C.; Wu, X. Ab initio theory and modeling of water. *Proc. Nat. Acad. Sci.* **2017**, *114*, 10846–10851.

(48) Tribello, G. A.; Bonomi, M.; Branduardi, D.; Camilloni, C.; Bussi, G. PLUMED2: New feathers for an old bird. *Comp. Phys. Commun.* **2014**, *185*, 604–613.

(49) Parrinello, M.; Polino, D. Kinetics of Aqueous Media Reactions via Ab Initio Enhanced Molecular Dynamics: The Case of Urea Decomposition. *J. Phys. Chem. B* **2019**, *123*, 6851–6856.

(50) Biswas, S.; Wong, B. M. Ab initio metadynamics calculations reveal complex interfacial effects in acetic acid deprotonation dynamics. *J. Mol. Liq.* **2021**, *330*, 115624.

(51) Branduardi, D.; Bussi, G.; Parrinello, M. Metadynamics with adaptive Gaussians. *J. Chem. Theory Comput.* **2012**, *8*, 2247–2254.

(52) Yanai, T.; Tew, D. P.; Handy, N. C. A new hybrid exchange–correlation functional using the Coulomb-attenuating method (CAM-B3LYP). *Chem. Phys. Lett.* **2004**, *393*, 51–57.

(53) Svoboda, O.; Kubelova, L.; Slavicek, P. Enabling forbidden processes: Quantum and solvation enhancement of nitrate anion UV absorption. *J. Phys. Chem. A* **2013**, *117*, 12868–12877.

(54) Svoboda, O.; Slavicek, P. Is Nitrate Anion Photodissociation Mediated by Singlet–Triplet Absorption? *J. Phys. Chem. Lett.* **2014**, *5*, 1958–1962.

(55) Weigend, F.; Ahlrichs, R. Balanced basis sets of split valence, triple zeta valence and quadruple zeta valence quality for H to Rn: Design and assessment of accuracy. *Phys. Chem. Chem. Phys.* **2005**, *7*, 3297–3305.

(56) Neese, F.; Wennmohs, F.; Becker, U.; Riplinger, C. The ORCA quantum chemistry program package. *J. Chem. Phys.* **2020**, *152*, 224108.

(57) Riikonen, S.; Parkkinen, P.; Halonen, L.; Gerber, R. B. Ionization of Acids on the Quasi-Liquid Layer of Ice. *J. Phys. Chem. A* **2014**, *118*, 5029–5037.

(58) Gerber, R. B.; Varner, M. E.; Hammerich, A. D.; Riikonen, S.; Murdachaew, G.; Shemesh, D.; Finlayson-Pitts, B. J. Computational Studies of Atmospherically-Relevant Chemical Reactions in Water Clusters and on Liquid Water and Ice Surfaces. *Acc. Chem. Res.* **2015**, *48*, 399–406.

(59) de la Puente, M.; David, R.; Gomez, A.; Laage, D. Acids at the Edge: Why Nitric and Formic Acid Dissociations at Air–Water Interfaces Depend on Depth and on Interface Specific Area. *J. Am. Chem. Soc.* **2022**, *144*, 10524–10529.

(60) Kang, H. Chemistry of ice surfaces. Elementary reaction steps on ice sutdeied by reactive ion scattering. *Acc. Chem. Res.* **2005**, *38*, 893—-900.

(61) Park, S.-C.; Kim, J.-K.; Lee, C.-W.; Moon, E.-S.; Kang, H. Acid–Base Chemistry at the Ice Surface: Reverse Correlation Between Intrinsic Basicity and Proton-Transfer Efficiency to Ammonia and Methyl Amines. *ChemPhysChem* **2007**, *8*.

(62) Hudait, A.; Allen, M. T.; Molinero, V. Sink or Swim: Ions and Organics at the Ice–Air Interface. *J. Am. Chem. Soc.* **2017**, *139*, 10095–10103.

(63) Harris, L. The lower electronic states of nitrite and nitrate ion, nitromethane, nitramide, nitric acid, and nitrate esters. *J. Chem. Phys.* **1973**, *58*, 5615–5626.

(64) McCarthy, M. I.; Peterson, K. A.; Hess, W. P. Electronic structure of sodium nitrate: Investigations of laser desorption mechanisms. *J. Phys. Chem.* **1996**, *100*, 6708–6714.

(65) Lebrero, M. C. G.; Bikiel, D. E.; Elola, M. D.; Estrin, D. A.; Roitberg, A. E. Solvent-induced symmetry breaking of nitrate ion in aqueous clusters: A quantum-classical simulation study. *J. Chem. Phys.* **2002**, *117*, 2718–2725.

(66) Thøgersen, J.; Rehault, J.; Odelius, M.; Ogden, T.; Jena, N. K.; Jensen, S. J. K.; Keiding, S. R.; Helbing, J. Hydration dynamics of aqueous nitrate. *J. Phys. Chem. B* **2013**, *117*, 3376–3388.

(67) Yadav, S.; Choudhary, A.; Chandra, A. A first-principles molecular dynamics study of the solvation shell structure, vibrational spectra, polarity, and dynamics around a nitrate ion in aqueous solution. *J. Phys. Chem. B* **2017**, *121*, 9032–9044.

(68) Hullar, T. Personal Communication. **Jan. 22 2023**,

(69) Prlj, A.; Ibele, L. M.; Marsili, E.; Curchod, B. On the Theoretical Determination of Photolysis Properties for Atmospheric Volatile Organic Compounds. *J. Phys. Chem. Lett.* **2020**, *11*, 5418–5425.

(70) Thompson, T.; Tapavicza, E. First-Principles Prediction of Wavelength-Dependent Product Quantum Yields. *J. Phys. Chem. Lett.* **2018**, *9*, 4758–4764.

TOC Graphic